Waiting time distribution and current correlations via a Majorana single-charge transistor

Wei Fu,[1] Sha-Sha Ke,[1,*] Yong Guo,[2] Huai-Wu Zhang,[1] and Hai-Feng Lü[1,2,†]

[1]*School of Physics and State Key Laboratory of Electronic Thin Films and Integrated Devices,*
University of Electronic Science and Technology of China, Chengdu 610054, China

[2]*Department of Physics and State Key Laboratory of Low-Dimensional Quantum Physics, Tsinghua University, Beijing 100084, China*

We investigate the electron transport and the waiting time distribution (WTD) in a topological superconducting Coulomb island system weakly coupled to two metallic leads. A pair of Majorana bound states are hosted in the island with a finite charging energy. By employing the Markovian master equation, we study the effect of interplay between Majorana energy splitting and the charging energy on the current correlations and the relevant electron WTDs. It is found that the super-Poissonian shot noise could be induced when the Majorana energy splitting is larger than the charging energy. The reason is that the degeneracy of the ground states in the island could be lifted by a finite Majorana energy splitting, which produces the asymmetry between tunneling channels and leads to the dynamical channel blockade effect. We show that the WTD for electron tunneling through two Majorana bound states is equivalent to the WTD in a single-resonant-level device. For comparison, we also discuss the WTD for electron tunneling through a non-Majorana device. It is found that the WTD sensitively depends on the length of the island and indicates oscillation behaviors in the absence of Majorana bound states. The particular behaviors of the WTDs in a Majorana island device can be useful in identifying the existence of Majorana bound states. Furthermore, we study the randomness parameter of the waiting time to describe the fluctuations of waiting times. It is shown that the randomness parameter indicates behavior similar to that indicated by the noise Fano factor, and both of them reflect the information of tunneling dynamics.

I. INTRODUCTION

The search for Majorana bound states (MBSs) at the edges of one-dimensional topological superconductors or the chains of adatoms on superconducting substrates has attracted increased attention recently, due to expected applications in topological quantum computation [1–4]. Possible signatures supporting the existence of such modes have already been reported by several experiments [5–11]. Another important aspect making such hybrid systems interesting is that the quantum transport in the presence of Majorana modes could indicate several unique and important tunneling signatures [12,13]. For instance, the coupling to a topological superconductor hosting Majorana quasiparticles results in the zero-bias conductance peak [12]. As the signature of the MBSs, the zero-bias conductance peak has been observed in hybrid devices of superconductor and semiconductor nanowire [14,15] and in ferromagnetic iron atomic chains on the surface of a superconductor [6]. In an interacting transistor with MBSs, it is found that the conductance shows Coulomb oscillations with universal halving of the finite-temperature peak conductance under strong blockade conditions [16,17]. Despite the fact that several experiments using such platforms have reported signatures compatible with MBSs, the Majorana interpretation has been challenged because zero-

energy Andreev bound states, in the absence of an underlying topological state, can mimic MBSs [18–22]. The most recent experiments demonstrate that the appearance of the robust zero-bias peaks in tunneling spectroscopy is more likely induced by trivial Andreev levels in the Yu-Shiba-Rusinov regime, while not originating from Majorana zero modes [20,23,24]. At this stage, it is urgent to search for a signal that can provide an alternative or confirmative proof to verify the existence of MBSs.

Quantum statistical properties of charge transfer in mesoscopic devices can be described by full counting statistics (FCS) [25,26]. The FCS in a long-time limit captures statistical information about the low-frequency fluctuations of the number of transferred charges, providing the average current, the zero-frequency noise, and higher-order current cumulants. The finite-time FCS has been developed to access short-time physics [27,28]. In addition, the waiting time distribution (WTD) represents the probability distribution of the time interval between two successive electrons transmitted through a conductor, which can also serve as a useful tool for describing short-time fluctuations in quantum nanoscale systems [29–35].

Theoretically, Brandes [36] firstly discussed the WTD and its relation to other statistical transport quantities in single-particle transport using the quantum master equations. The WTD has been investigated to understand the short-time dynamics of various systems with electron-electron interactions [37–39], electron-phonon interactions [40], non-Markovian quantum transport [30], Cooper pair splitting [41,42], and spintronics [29]. For instance, it was found that the statistics of

*keshasha@uestc.edu.cn
†lvhf04@uestc.edu.cn

the WTD can be used to characterize Cooper pair splitters that create spatially separated spin-entangled electrons [41,43]. A short waiting time between tunneling events in which electrons tunnel into different leads is associated with the fast emission of a split Cooper pair, while long waiting times are governed by the slow injection of Cooper pairs from a superconductor [41]. In addition, a scattering matrix formalism has been developed to evaluate the WTDs in fully coherent transport systems [44–48]. The WTD taking into account the higher-order processes for electron transport through an interacting quantum dot has been recently investigated [38,49]. Experimentally, measurements of microscopic current fluctuations and waiting times between tunneling events have been realized in various quantum devices [50–52]. Spurred by the rapid development of real-time single-electron detection techniques [50,53–56], the WTDs in a dynamic single-electron transistor has been measured recently [51]. The observed WTDs are quite different from that corresponding to a Poisson process and can be well explained by the theoretical analysis [51]. By detecting the time-resolved statistics including the WTD, it has been demonstrated that strong nonlocal correlations exist in Cooper pair splitters [52]. The WTD indicates different features as a function of bias voltage in the junctions made of s-wave or p-wave superconductors [46]. Although conductance properties in Majorana devices have been widely explored [13,16,57–63], the WTD is much less studied [46].

In this paper, we investigate the WTD and current correlations in a Majorana single-charge transistor. Such devices have been realized in a semiconducting nanowire partially covered by or fully wrapped in a superconducting shell, and Majorana modes can be obtained by applying proper magnetic fields [5,20,64]. It is expected that the nonlocal current correlations and the WTD contain the extra dynamical information mediated by the interaction between the Majorana energy splitting and the charging energy in a Majorana island. The paper is organized as follows. In Sec. II, we introduce the model Hamiltonian of the Majorana single-charge device, as well as the formulas to calculate the Fano factor and the WTD. In Sec. III, we investigate the nonlocal transport and the WTD properties modulated by the charging energy and the Majorana energy splitting in the island. As a comparison, we also study the WTD in a non-Majorana island device. Finally, a summary is given in Sec. IV.

II. MODEL AND FORMULA

A. Model Hamiltonian

As schematically shown in Fig. 1, we consider a Coulomb-blockaded topological superconducting quantum nanowire hosting a pair of MBSs at its two ends weakly coupled to two metallic leads (the source and drain). The coupling between the two MBSs can be modeled by the following Hamiltonian:

$$H_d = \epsilon_M d^\dagger d, \qquad (1)$$

where ϵ_M is the Majorana splitting energy. Majorana operators γ_i ($i = L, R$) describing the two spatially separated Majorana excitations satisfy $\gamma_i = \gamma_i^\dagger$. They can be combined into a usual nonlocal fermion operator d, $d = (\gamma_L + i\gamma_R)/\sqrt{2}$. If the length of the quantum wire is comparable to the size of the
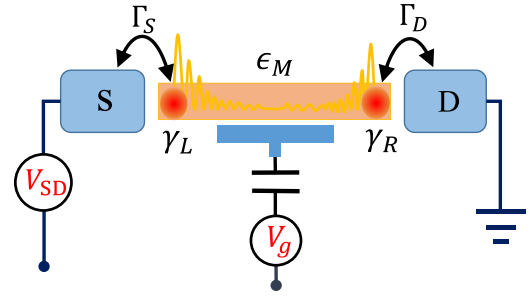

FIG. 1. Schematic of the setup: A topological superconductor (TS) Coulomb island hosting MBSs at the two ends with the energy splitting ϵ_M is weakly coupled to two metallic leads (the source and drain). The Coulomb interacting effect is included by giving the charging energy $E_c = e^2/2C$.

wave packet of two Majorana states, the formed fermionic mode gains a finite energy splitting ϵ_M due to the overlapping of their wave functions. It is shown that the energy splitting decreases exponentially as a function of the length of the quantum wire as long as MBSs are exponentially localized [65].

In our setup, the Cooper pair number of a floating topological superconducting nanowire is allowed to fluctuate, and the Coulomb interaction on the topological nanowire is included via the charging energy $E_c = e^2/2C$ [17]. The instantaneous charge state of the superconducting island is specified by the occupation of the d fermionic mode and the number of Cooper pairs. Such a charge state can be represented as $|Q\rangle \equiv |N, n_d\rangle$, where N and n_d are the eigenvalue of Cooper pair number operator $\hat{N}$ and d-fermion number operator $\hat{n}_d = d^\dagger d$, respectively. Then, the Coulomb interaction is effectively described by the Hamiltonian

$$H_c = E_c(2\hat{N} + \hat{n}_d - n_g)^2, \qquad (2)$$

where $n_g \in \mathcal{R}$ can be tuned by a gate voltage.

The source and drain are noninteracting electron reservoirs with Hamiltonian

$$H_l = \sum_{\alpha,k} \epsilon_{\alpha k} c_{\alpha k}^\dagger c_{\alpha k}, \qquad (3)$$

where $\alpha = \{S, D\}$ labels the source and drain electrode, $\epsilon_{\alpha k} = \epsilon_k + \mu_\alpha$ with μ_α being the chemical potential of lead α, and $c_{\alpha k}^\dagger$ is the lead electron creation operator with energy ϵ_k. Here, we should note that electrons in leads are effectively modeled as spinless fermions when we consider electron transport through nanowire by mediating MBSs at the two ends [66].

The electron tunneling between two leads and nanowire is described by the following Hamiltonian [16,67]:

$$H_t = \frac{1}{\sqrt{2}} \sum_{\alpha=\{S,D\},k} \lambda_\alpha c_{\alpha k}^\dagger (d + s_\alpha e^{-i\phi} d^\dagger) + \text{H.c.}, \qquad (4)$$

where $s_S = 1$ ($s_D = -1$), λ_α is the momentum-independent tunneling amplitude, ϕ is the superconductor condensate phase which is the conjugate variable to $\hat{N}$, $[\phi, \hat{N}] = i$. Since $e^{\pm i\phi}$ creates or breaks a Cooper pair in the superconducting island, the tunnel Hamiltonian preserves the charge

conservation. Finally, the Hamiltonian of the system can be written as $H = H_d + H_c + H_l + H_t$.

B. Transition rates and n-resolved master equation

In this paper, we investigate the electron transport across a Majorana island device in the weak-tunneling regime where the tunneling coupling strength $\Gamma_\alpha = \pi |\lambda_\alpha|^2 \nu_\alpha$, with ν_α being the density of states in lead α, is much smaller than Δ and E_c. One of main approaches is based on the quantum master equation. It is the equation of motion of the reduced density $\rho_{\text{island}}(t) = \text{Tr}_{\text{leads}}[\rho(t)]$, where the trace is over electronic states of the leads and $\rho(t)$ is the density operator of the total system. In our present system, since there is a one-to-one correspondence between the island charge state $|Q\rangle$ and the charge number $Q = 2N + n_d$, we can write the charge state as $|Q\rangle = |N, n_d\rangle$. In the secular approximation, the nondiagonal entries of ρ_{island} are assumed to decay rapidly and can be neglected [38,68]. The diagonal elements $P_Q \equiv [\rho_{\text{island}}]_{QQ} = \langle Q | \rho_{\text{island}} | Q \rangle$ describe the occupation probabilities of the charge states. The master equation of ρ_{island} then is reduced to the rate equations for P_Q, which can be constructed from the transition rates between different charge states. In the following, we adopt the T-matrix formalism to obtain the transition rates up to the fourth order in the tunneling amplitude. For $k_B T, eV \gg \Gamma_\alpha$ and in the Coulomb blockade regime, the T-matrix approach has been shown to be a reasonable approximation to calculate the transition rates under the Markov assumption [38,68].

The transition amplitude from an initial charge state $|i\rangle$ at $t = t_0$ to a final state $|f\rangle$ at the time t is given by $\langle f | i(t) \rangle$, and the corresponding transition rate can be defined as

$$\Gamma_{fi}(t) \equiv \frac{d}{dt} |\langle f | i(t) \rangle|^2. \tag{5}$$

In the T-matrix formalism, one can define the following T matrix in a recursive way [69]:

$$
\begin{aligned}
T &= H_t + H_t \frac{1}{E_i - H_0 + i0} T \\
&= H_t + H_t \frac{1}{E_i - H_0 + i0} H_t + O(H_t^3), \tag{6}
\end{aligned}
$$

where E_i is the energy of an initial state when the tunneling is turned off and $H_0 = H_c + H_l + H_d$ describes the decoupled leads and Majorana island in our present case. The transition rate equation (5) can be expressed as a form of generalized Fermi's golden rule

$$\Gamma_{fi} = 2\pi \langle f | T | i \rangle|^2 \delta(E_f - E_i), \tag{7}$$

where E_f (E_i) is the eigenenergy of the final state $|f\rangle$ (initial state $|i\rangle$) and the δ function indicates the energy conservation.

In order to get the transition rates among various island charge states, we take the state $|i\rangle$ ($|f\rangle$) as a tensor product state of the island charge state $|Q\rangle$ ($|Q'\rangle$) and continuous lead states $|i_l\rangle$ ($|f_l\rangle$). The lowest-order term of H_t in the expansion of the T matrix describes the sequential tunneling processes with a single electron tunneling between the island and one of the two leads. Here, we rewrite $H_t = \sum_{\alpha=S,D} H_{\alpha t}$ with $H_{\alpha t}$ describing the electron tunneling between the island and lead α. The sequential tunneling rates for the electron tunneling

through lead j can be expressed as

$$
\begin{aligned}
\Gamma_{\alpha, Q', Q} = 2\pi \sum_{f_\alpha, i_\alpha} |\langle f_\alpha | \langle Q' | H_{\alpha t} | Q \rangle | i_\alpha \rangle|^2 W_{i_\alpha, Q} \\
\times \delta\big(E(Q') + \epsilon_{f_\alpha} - E(Q) - \epsilon_{i_\alpha}\big), \tag{8}
\end{aligned}
$$

where $W_{i_\alpha, Q}$ is the thermal distribution function for the lead α with state $|i_\alpha\rangle$. Note that the summation in Eq. (8) should be replaced by the integration when we consider continuous lead states. After integrating out continuous electronic states of the lead, we get the corresponding transition rate

$$\Gamma^{(\text{Seq})}_{\alpha, Q\pm1, Q} = \frac{\Gamma_i}{2} n_F(E(Q \pm 1) - E(Q) + (-1)^Q \epsilon_M \mp \mu_\alpha), \tag{9}$$

where $Q = 2N + n_d$ is the charge number of the island state $|Q\rangle$, $E(Q) = E_c(Q - n_g)^2$, and $n_F(\epsilon) = 1/(e^{\beta\epsilon} + 1)$ with $\beta = 1/k_B T$ is the Fermi-Dirac distribution function.

More complicated cotunneling processes are included in the next-to-leading term in the T-matrix expansion of H_t. In our considered parameter regime, the topological superconducting gap dominates all other energy scales, i.e., $\Delta \gg E_C, \epsilon_M, \Gamma_{S/D}$, and the rates of cotunneling processes via states above the superconducting gap are suppressed by a factor of $1/\Delta$ [16]. All cotunneling processes except those involving the superconductor ground state and MBSs are ignored. For the present case of a Majorana island, cotunneling processes fall into two classes: inelastic and elastic cotunneling processes. Elastic cotunneling processes involve electron transfer from lead S (D) to D (S) through the island and preserve the energy of the island state. When $\epsilon_M \neq 0$, this means that elastic cotunneling processes will leave the island state unchanged. Inelastic cotunneling processes correspond to the local or crossed Andreev reflections. For a local Andreev reflection, an electron and a hole tunneling from the same lead form a Cooper pair on the island; for the crossed Andreev reflection, the formed Cooper pair comes from an electron and a hole of different leads. Their inverse processes include those processes which split a Cooper pair [16] and transfer the electrons into leads. Here, we defer the detailed derivations of the regularized cotunneling rates to the Appendix.

To perform the calculations of the current correlations and WTDs, we employ the n-resolved master equation. It is based on the n-resolved occupation probability for the Majorana island charge states. Here, we define $P_Q(n, t)$ as the probability of the island in the charge state Q with n electrons having been transported from the source to the drain in time interval $[0, t]$. The n-resolved Markovian master equation can be written as the following matrix form:

$$\frac{d\mathbf{P}(n, t)}{dt} = \sum_{n'} \mathbf{M}(n - n') \mathbf{P}(n', t), \tag{10}$$

where $\mathbf{P}(n, t)$ is defined as

$$\mathbf{P}(n, t) = (\ldots, P_{Q-1}(n, t), P_Q(n, t), P_{Q+1}(n, t), \ldots)^{\text{T}}. \tag{11}$$

If we consider both sequential and cotunneling processes, the sum over n' includes only five terms with $n - n' = 0, \pm 1, \pm 2$.

Then, we rewrite Eq. (10) as

$$\frac{d\mathbf{P}(n,t)}{dt} = \mathbf{M}_0\mathbf{P}(n,t) + \mathbf{J}_{\pm 1}\mathbf{P}(n \mp 1,t) + \mathbf{J}_{\pm 2}\mathbf{P}(n \mp 2,t),$$

$$(12)$$

where the matrices $\mathbf{M}_0$, $\mathbf{J}_{\pm 1}$, and $\mathbf{J}_{\pm 2}$ can be constructed from the sequential tunneling rates and the regularized co-tunneling rates. Instead of solving the n-resolved master equation directly, it is useful to Fourier-transform Eq. (10) to the counting-field χ space. In χ space, the master equation becomes [40]

$$\frac{d\tilde{\mathbf{P}}(\chi,t)}{dt} = \tilde{\mathbf{M}}(\chi)\tilde{\mathbf{P}}(\chi,t), \tag{13}$$

where

$$\tilde{\mathbf{P}}(\chi,t) = \sum_n \mathbf{P}(n,t)e^{in\chi} \tag{14}$$

and

$$\tilde{\mathbf{M}}(\chi) = \sum_{n'} e^{i(n'-n)\chi}\mathbf{M}(n'-n)$$

$$= \mathbf{M}_0 + \sum_{k=\pm 1,\pm 2} \mathbf{J}_k e^{ik\chi}. \tag{15}$$

Due to the time independence of $\tilde{\mathbf{M}}(\chi)$, the form solution of Eq. (13) can be written as

$$\tilde{\mathbf{P}}(\chi,t) = e^{\tilde{\mathbf{M}}(\chi)t}\tilde{\mathbf{P}}(\chi,0), \tag{16}$$

with $\tilde{\mathbf{P}}(\chi,0)$ being the initial probability distribution in χ space. Because the electron-counting processes are assumed to start at $t = 0$ when the system stays at a stationary state, we have $\mathbf{P}(n \neq 0, 0) = 0$ and $\tilde{\mathbf{P}}(\chi,0) = \mathbf{P}(n = 0, 0)$. In the following, we set $\mathbf{P}^{(0)} = \tilde{\mathbf{P}}(\chi,0)$, and $\mathbf{P}^{(0)}$ satisfies the equation $\mathbf{M}\mathbf{P}^{(0)} = 0$ with $\mathbf{M} \equiv \mathbf{M}(\chi = 0)$. The $\mathbf{P}(n,t)$ can be obtained by performing the inverse Fourier transform:

$$\mathbf{P}(n,t) = \frac{1}{2\pi}\int_0^{2\pi} e^{-in\chi}e^{\tilde{\mathbf{M}}(\chi)t}\mathbf{P}^{(0)}d\chi. \tag{17}$$

The distribution for the charge transfer at time t is given by

$$P(n,t) = (\mathbf{I}, \mathbf{P}(n,t)) = \sum_Q P_Q(n,t), \tag{18}$$

where $\mathbf{I}$ is the identity vector.

C. Current and noise correlations

The stationary transport properties of a system are determined by the normalized occupation probability $\mathbf{P}^{(0)}$. For a floating Majorana island device, we have current conservation $I_S = -I_D$. Here, the current flowing into the drain can be cast in the form [70]

$$I_D = e\sum_Q [\mathbf{J}_D\mathbf{P}^{(0)}]_Q, \tag{19}$$

where $\mathbf{J}_D$ is the matrix of the current operator. In our present case, $\mathbf{J}_D$ is given by

$$\mathbf{J}_D = \sum_k k\mathbf{J}_k, \tag{20}$$

where we define the current to be positive for an electron transfer from the island to the drain. Similarly, we can construct a current matrix $\mathbf{J}_S$ for the source electrode.

The Wiener-Khinchin theorem shows that the noise spectrum $S(\omega)$ is related to the current correlation function via

$$S_{\alpha\beta}(\omega) = 2\int_{-\infty}^{+\infty} dt\, e^{i\omega t}[\langle I_\alpha(t)I_\beta(0)\rangle - \langle I\rangle^2], \tag{21}$$

where $\langle\cdot\rangle$ is the average over the time. To convert this time average into an average over the initial steady-state occupation probabilities, we introduce a time-evolution operator $\mathbf{T}(t) \equiv e^{\mathbf{M}t}$. Then, the current-current correlation function in Eq. (21) can be expressed in terms of the current operators and the time-evolution operator as [70]

$$\langle I_\alpha(t)I_\beta(0)\rangle = \theta(t)\sum_Q[\mathbf{J}_\alpha\mathbf{T}(t)\mathbf{J}_\beta\mathbf{P}^{(0)} + \mathbf{J}_\beta\mathbf{T}(-t)\mathbf{J}_\alpha\mathbf{P}^{(0)}]_Q$$

$$+ e\delta_{\alpha\beta}\delta(t)\sum_Q |[\mathbf{J}_\alpha\mathbf{P}^{(0)}]_Q|, \tag{22}$$

where $\theta(t)$ is the Heaviside function. After a Fourier transform to ω space, we can get the noise spectrum. In the limit of $\omega \to 0$, the noise spectra for the cross-correlation and autocorrelation of the currents are equal. Here, we take $S(0) \equiv S_{SD}(0)$, and the dimensionless Fano factor F is defined as

$$F = \frac{S(0)}{2e\langle I_D\rangle}. \tag{23}$$

D. Waiting time distribution

The electron waiting time is the time delay between two subsequent electron emissions into the given one or two leads. Here, we consider the WTDs for electrons jumping into the drain electrode. Recently, the electron WTDs in an interaction quantum dot including higher-order effects has been explored in the framework of real-time diagrammatic theory [49]. It has been shown that the effects of higher-order tunneling processes on the WTDs will be strongly suppressed with the increase in electronic temperature [49]. In the following, for relatively high temperature and large bias, we evaluate the WTDs in the sequential tunneling regime, using the n-resolved master equation with the transition rates obtained in Sec. II B. After introducing the idle time probability $\Pi(\tau)$, which is the probability that no transported electron has been detected in the drain during a time interval τ [71], the conditional WTD is defined as

$$w(\tau) = \langle\tau\rangle\frac{\partial^2}{\partial\tau^2}\Pi(\tau), \tag{24}$$

where the mean waiting time $\langle\tau\rangle$ is given by

$$\langle\tau\rangle = \int_0^\infty w(\tau)\tau d\tau = -\frac{1}{\dot{\Pi}(\tau)|_{\tau=0}}. \tag{25}$$

Based on the n-resolved occupation probability, the idle time probability $\Pi(\tau)$ can be identified as $P(n = 0, \tau)$ [38]. In the large-bias limit, combining with the definition of $\tilde{\mathbf{M}}(\chi)$ given in Eq. (14), we exclude all back-tunneling terms and get

$$\tilde{\mathbf{M}}(\chi) = \mathbf{M}_0 + \mathbf{J}e^{i\chi}, \tag{26}$$

where $\mathbf{J} = \mathbf{J}_1$. The idle time probability can be written as

$$\Pi(\tau) = \lim_{\chi \to i\infty} (\mathbf{I}, e^{\tilde{\mathbf{M}}(\chi)\tau} \mathbf{P}^{(0)}). \tag{27}$$

Plugging Eq. (27) into Eq. (24), we obtain

$$w(\tau) = -\lim_{\chi \to i\infty} \frac{(\mathbf{I}, \tilde{\mathbf{M}}(\chi) e^{\tilde{\mathbf{M}}(\chi)\tau} \tilde{\mathbf{M}}(\chi) \mathbf{P}^{(0)})}{(\mathbf{I}, \tilde{\mathbf{M}}(\chi) \mathbf{P}^{(0)})}. \tag{28}$$

Finally, using the explicit form of $\tilde{\mathbf{M}}(\chi)$ given by Eq. (26), we get [38]

$$w(\tau) = \frac{(\mathbf{I}, \mathbf{J} e^{\mathbf{M}_0 \tau} \mathbf{J} \mathbf{P}^{(0)})}{(\mathbf{I}, \mathbf{J} \mathbf{P}^{(0)})}. \tag{29}$$

In Laplace space, the WTD reads

$$\tilde{w}(z) = \frac{(\mathbf{I}, \mathbf{J}(z - \mathbf{M}_0)^{-1} \mathbf{J} \mathbf{P}^{(0)})}{(\mathbf{I}, \mathbf{J} \mathbf{P}^{(0)})}. \tag{30}$$

The moment-generating function of $w(\tau)$ is defined as

$$G(z) = \int_0^\infty d\tau \, e^{iz\tau} w(\tau) = -\frac{(\mathbf{I}, \mathbf{J}(\mathbf{M}_0 + iz)^{-1} \mathbf{J} \mathbf{P}^{(0)})}{(\mathbf{I}, \mathbf{J} \mathbf{P}^{(0)})}. \tag{31}$$

The moments of τ can be obtained by taking derivatives of Eq. (31) with respect to z and are explicitly given by

$$\langle \tau^n \rangle = \int_0^\infty d\tau \, \tau^n w(\tau)$$
$$= n!(-1)^{n+1} \frac{(\mathbf{I}, \mathbf{J} \mathbf{M}_0^{-(n+1)} \mathbf{J} \mathbf{P}^{(0)})}{(\mathbf{I}, \mathbf{J} \mathbf{P}^{(0)})}. \tag{32}$$

III. RESULTS AND DISCUSSION

In this section we discuss the subgap electron transport in the weak-tunneling regime where the superconducting energy gap Δ is much larger than other energy scales, i.e., $\Delta \gg E_c, \epsilon_M, \Gamma_{S/D}$. In this regime, the electron transport through the island is dominated by subgap MBSs and Andreev reflections. Here, we consider the case that the superconducting island is floating and the setup is a two-terminal device. In this case, the superconducting island behaves like a Cooper pair box with multiple interacting energy levels. Majorana energy splitting ϵ_M and the charging energy E_c are two competing parameters that determine electron transport properties. In the following discussion, we focus on the shot noise and the WTD properties of the electron transport through the Majorana island. In the calculation, we adopt the symmetric lead-island coupling strength $\Gamma_{S/D} = \Gamma/2$ for simplicity. We choose $\mu_S = -\mu_D = eV_{SD}/2$ and $k_B T = 2.5\Gamma$. The shot noise reflects the dynamical tunneling correlations and is frequency dependent, which is different from the Schottky noise [72]. In addition, the WTDs and related randomness parameter are calculated to reveal more information about time-resolved dynamics.

A. Current, conductance, and Fano factor

We start by studying the case where the Majorana energy splitting ϵ_M is exact zero. Figure 2 summarizes the dependence of the current, the conductance, and the noise Fano
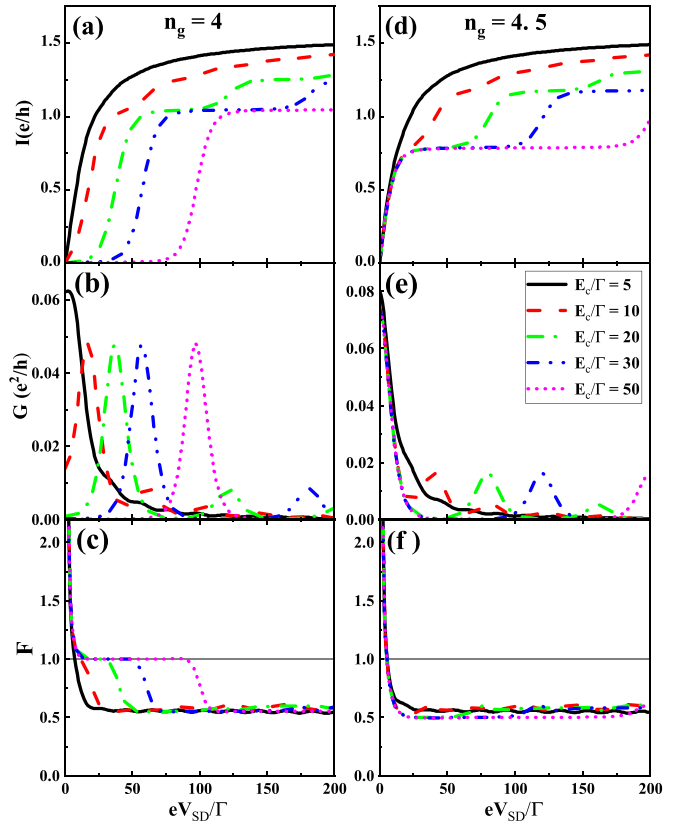

FIG. 2. (a) and (d) The steady-state current I, (b) and (e) conductance G, and (c) and (f) Fano factor F as functions of bias voltage V_{SD} with different Coulomb charging energies for $n_g = 4.0$ and $n_g = 4.5$, respectively. The Majorana island hosts a pair of zero-energy MBSs.

factor on the applied bias voltage V_{SD} for different values of E_c with $n_g = 4.0$ and $n_g = 4.5$, respectively. For the case where n_g is an integer or half-integer, the energy spectra of the Majorana island are different. When n_g is an integer, the ground state of system is nondegenerate, and all excited states are doubly degenerated; for a half-integer n_g, all energy levels including the ground state are doubly degenerated. We first discuss the case in which n_g is an integer. When the bias voltage is lower than $2E_c$, the electron transport is dominated by thermally activated sequential tunneling and cotunneling processes. In the Coulomb blockade regime, the first-order tunneling is exponentially suppressed, while the higher-order processes can contribute a small current. As illustrated in Figs. 2(a) and 2(b), the tunneling channel related to the first excited states is open, and a conductance peak appears near $eV_{SD} = 2E_c$. In the low-bias regime with $eV_{SD} \ll k_B T$, the shot noise is mainly induced by thermal fluctuations, and the noise Fano factor is divergent in this case. With the increase in bias voltage, the electron tunneling through the device becomes independent events for $eV_{SD} < 2E_c$, leading to a Poissonian shot noise with the Fano factor $F = 1$. In the large-bias regime, more eigenenergy levels of the Majorana island enter the transport window. Having multiple energy levels participating in transport weakens the competition or cooperation between different tunneling channels, resulting in a sub-Poissonian Fano factor which is close to $1/2$. The Fano factor $F = 1/2$ has been found in noninteracting fermion
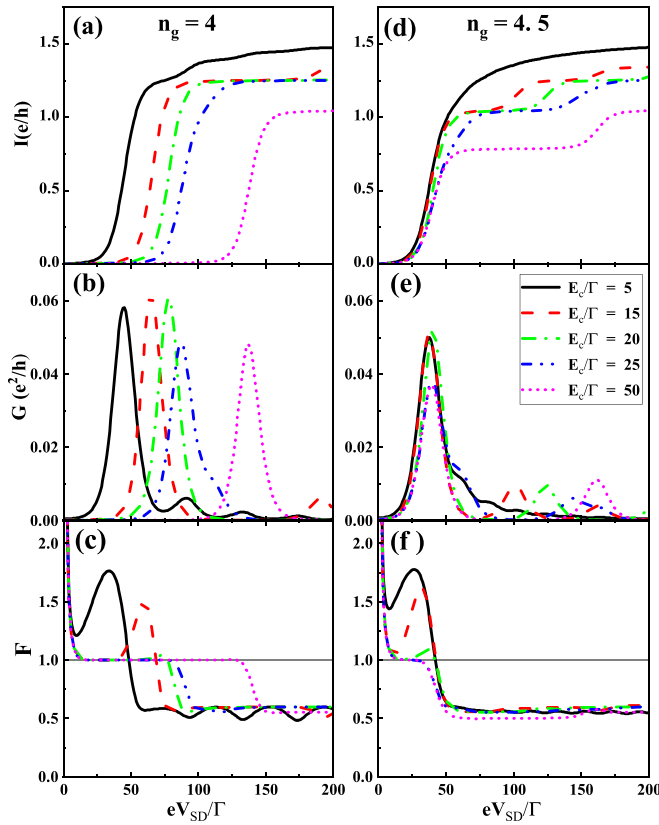
FIG. 3. We take the Majorana energy splitting $\epsilon_M = 20\Gamma$. (a) and (d) The steady-state current I, (b) and (e) conductance G, and (c) and (f) Fano factor F are plotted as functions of bias voltage V_{SD} with different Coulomb charging energies for $n_g = 4.0$ and $n_g = 4.5$.

FIG. 4. (a) and (d) The steady-state current I, (b) and (e) conductance G, and (c) and (f) Fano factor F as functions of bias voltage V_{SD} with serious values of Majorana energy splitting for $n_g = 4.0$ and $n_g = 4.5$. The Majorana island charging energy is $E_c = 20\Gamma$.

transport systems and in the symmetric single-electron transistor in the high-bias regime [72]. When n_g is a half-integer, the sequential tunneling processes dominate electron transport in the whole bias regime. In this case, a zero-bias conductance peak always exists, as shown in Figs. 2(d) and 2(e). In addition, the sideband peaks appear at $eV_{SD} = 4E_c$, which means that a pair of states with higher energy enters the bias window. Different from the integer n_g case where a Fano factor plateau with $F = 1$ appears, the Fano factor for the half-integer n_g case exhibits a sub-Poissonian value ($F < 1$) in a wide range of bias voltages.

Next, we consider the effects of a finite Majorana energy splitting on the transport properties. The finite Majorana energy splitting can considerably modulate the energy spectrum of the Majorana island, and the degeneracy of energy levels is partly lifted. This dependence remarkably modifies the electronic occupations in comparison with the noninteracting case. In Fig. 3, we take $\epsilon_M = 20\Gamma$ and plot the current, the conductance, and the Fano factor as a function of bias voltage V_{SD} for several values of E_c. For $n_g = 4$, it is shown that the zero-bias conductance peak is shifted to $eV_{SD} = 2(E_c + \epsilon_M)$ because the energy difference between the ground state and the first excited state becomes $E_c + \epsilon_M$. For the case of $n_g = 4.5$, it is shown in Fig. 3(e) that there is no zero-bias conductance peak in the presence of a finite Majorana energy splitting. In this case, the degeneracy of energy levels is completely lifted. The energy gap between the ground state and
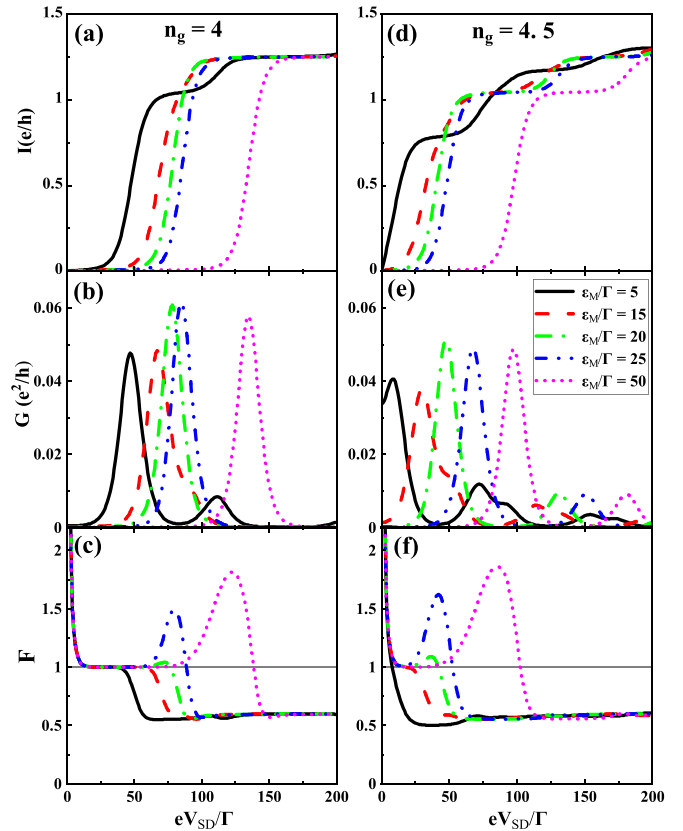
the first excited state is ϵ_M and independent of E_c, leading to a conductance peak appearing at $eV_{SD} = 2\epsilon_M$. As illustrated in Figs. 3(c) and 3(f), a finite Majorana energy splitting could induce a super-Poissonian shot noise with $F > 1$. This is similar to the single-level quantum dot device. When the spin degeneracy in the dot is lifted by applying a magnetic field and the chemical potentials of leads are properly adjusted, a super-Poissonian shot noise can be induced. In mesoscopic quantum devices, the super-Poissonian shot noise is usually induced by the dynamical channel blockade effect [73]. This mechanism has been illustrated in several quantum transport systems, such as multilevel quantum dot devices, Franck-Condon blockade in single molecules [74], and nanoscale oscillators. In the case of $E_c < \epsilon_M$, the energy gap between the first excited state and second excited state is smaller than the gap between the ground state and the first excited state. However, the Coulomb effect reduces the occupation probability of these higher-level states. As a consequence, the competition between the two transport channels arises, leading to a super-Poissonian shot noise. As the bias voltage is further increased, the super-Poissonian shot noise directly develops into a sub-Poissonian type because more tunneling channels enter the transport window.

In the following, we vary the Majorana energy splitting and take a fixed charging energy $E_c = 20\Gamma$. The results are presented in Fig. 4. For both cases with $n_g = 4$ and $n_g = 4.5$, it is shown in Figs. 4(a) and 4(d) that the currents are
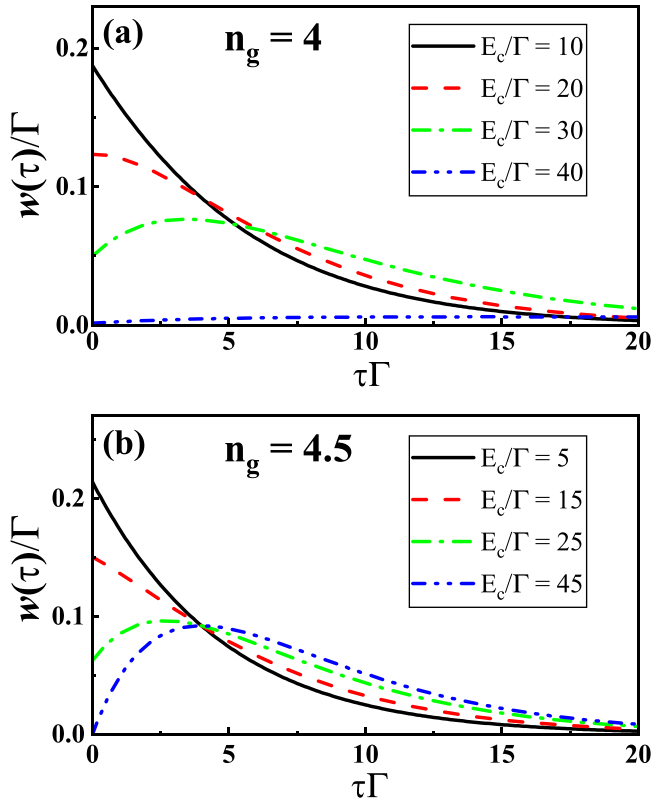
FIG. 5. (a) and (b) The WTDs for various charging energies with $\epsilon_M = 10\Gamma$. For a half-integer n_g and a large E_c, the WTD for electron transport through a Majorana island device takes the same form as that in a single-level quantum dot.

significantly suppressed in the low-bias-voltage regime with the increase in the Majorana energy splitting. As shown in Figs. 4(c) and 4(f), we find that the super-Poissonian shot noise exists more commonly under the condition $\epsilon_M > E_c$. In contrast, the sub-Poissonian shot noise appears in wide range of bias voltages for $\epsilon_M < E_c$. In the presence of the strong charging energy, the island prefers to occupy the ground state, and the occupation probabilities of other states are strongly suppressed. The long-time occupation of the ground state impedes the entry of electrons into the island region through other channels, leading to the suppression of the current and enhancement of shot noise when $\epsilon_M < E_c$.

B. Waiting time distributions in a Majorana single-charge transistor

In this section, we study the probability distribution of the electron waiting time between two successive electron jumps from the Majorana island into the drain. We choose the parameters $k_B T = 2.5\Gamma$, $\Gamma_{S/D} = \Gamma/2$, and $\mu_S = -\mu_R = 40\Gamma$ in the following calculations of the WTD. In this parameter regime, the bias is large enough compared with $k_B T$ to suppress the contributions from higher-order tunneling processes to the WTD but still small enough to limit the number of tunneling channels in the transport window to only a few.

In Fig. 5, we present the results of the WTDs with $\epsilon_M = 10\Gamma$ for various E_c. For a small E_c, the Cooper pair number is allowed to fluctuate when electrons transport through the

island. Electrons from the source can tunnel to the island with no need of overcoming the large Coulomb charging energy. Therefore the short waiting time has a relatively large probability distribution, and the maximum of the WTD appears at $\tau = 0$. As E_c increases, the tunneling of an electron into the Majorana island has a large Coulomb charging energy cost. In this case, the fluctuation in the Cooper pair number of the island is suppressed, and the charge states with high eigenenergy are removed from the transport window, giving rise to the broadening of WTDs. The waiting time with the maximum distribution also becomes longer in this case. In the large-E_c limit, we see that the WTD becomes very flat for an integer n_g due to the fact that there is no electron tunneling channel in the transport window. Electron tunneling to the drain can only be aided with thermal activated sequential tunneling processes which have exponentially reduced tunneling rates. Differently, when the charging energy is large and n_g is a half-integer, only two charge states with charge number differing by 1 remain in the transport window. In this situation, the Majorana island behaves like a single-level quantum dot system with a highly nonlocal electronic state, giving rise to phase-coherent electron teleportation even when the distance between two localized MBSs is much larger than the superconducting coherence length. This nonlocal property could result in a zero-bias conductance peak with a height of at most e^2/h [17]. Importantly, it can also be unraveled in the electron WTD. Using the master equation approach, the corresponding WTD is obtained and given by [36]

$$w(\tau) = \frac{\Gamma_S \Gamma_D}{\Gamma_D - \Gamma_S}(e^{-\Gamma_S \tau} - e^{-\Gamma_D \tau}). \tag{33}$$

Physically, right after an electron jumps into the drain, the nonlocal electronic state is left unoccupied, and it has to be reoccupied before the next electron can jump into the drain. Therefore the WTD is always suppressed at short times and starts from zero for $\tau = 0$, as shown in Fig. 5(b).

In order to study the effects of Majorana energy splitting on the WTD, we choose the charging energy $E_c = 25\Gamma$. The WTDs for different values of ϵ_M are plotted in Fig. 6. For different n_g, we find that the Majorana energy splitting can modulate the WTD nonmonotonically. Here, we first consider the case of $n_g = 4$. When ϵ_M is small, there are three states in the bias window, making the device a multiple reset system [36]. Thus the WTD gets a relatively large value at $\tau = 0$ and a short average waiting time. For a relatively large ϵ_M only the ground state stays in the bias window, leading to a large average waiting time. When $n_g = 4.5$, the Majorana island behaves more like a single-level quantum dot system for a small ϵ_M; see Fig. 6(b). As ϵ_M is increased, $w(0)$ enlarges, and the average waiting time becomes shorter. When $\epsilon_M > E_c$, we find that the corresponding WTDs take a maximum value at $\tau = 0$ and decay monotonically as the time elapses. We also see that similar WTDs show up in the case where E_c is small and multiple energy levels participate in the electron transport, as shown in Fig. 5.

The randomness parameter which is related to the Fano factor is defined as

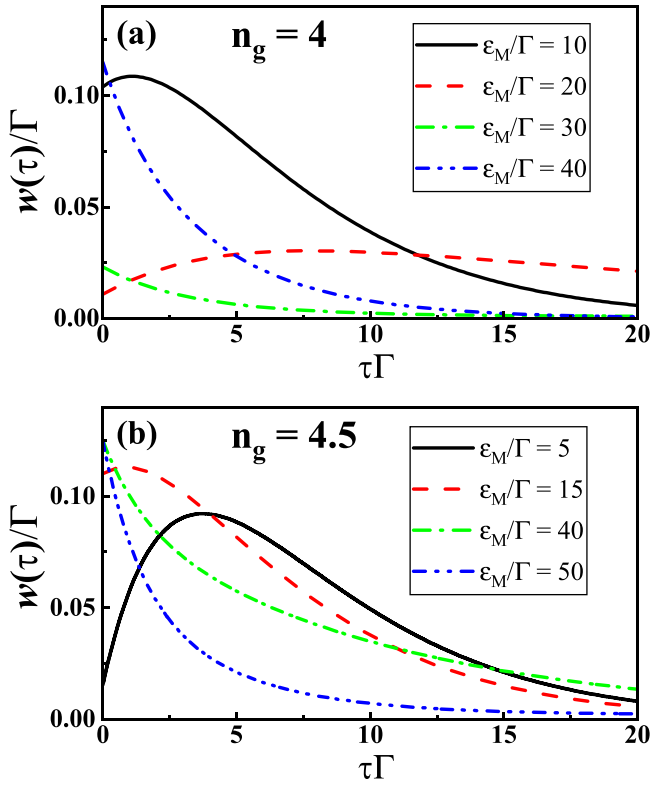$$R = \frac{\langle \tau^2 \rangle}{\langle \tau \rangle^2} - 1. \tag{34}$$

FIG. 6. (a) and (b) The WTDs for different Majorana energy splittings at fixed $E_c = 25\Gamma$.

If the electron transport processes satisfy the renewal assumption [75,76], it has been shown that the randomness parameter is equal to the noise Fano factor [77]. In Fig. 7, we plot the Fano factor and the randomness parameter as a function of bias voltage with $E_c = 30\Gamma$ for several values of ϵ_M. In the low-bias regime, we see that the Fano factor and the randomness parameter are equal for both cases. This originates from the fact that no or only one tunneling channel resides in the transport window, and the renewal assumption is well satisfied. As eV_{SD} increases, more channels start to enter the transport window. The discrepancy between the F and R arises because the electrons tunneling to the drain could take different channels, making successive waiting times correlated. In the large-bias limit, despite the difference between the two quantities, the sub-Poissonian transport property is still captured by the randomness parameter.

C. Comparison with a non-Majorana device

Above, we discuss the WTDs of electronic tunneling through a Majorana island. For strong charging energy, the electron transfer process by virtue of tunneling in and out of the MBSs manifests the nonlocal teleportation phenomenon [17]. In this case, a pair of MBSs are equivalent to a nonlocal single energy level, and the behavior of the WTD approaches to the result of a single-level quantum dot device with strong Coulomb interaction. This means that the WTDs in a Majorana island are irrelevant to the distance between two MBSs. For comparison, we turn to considering the WTD for electron transport through a nanowire island in the absence of MBSs,
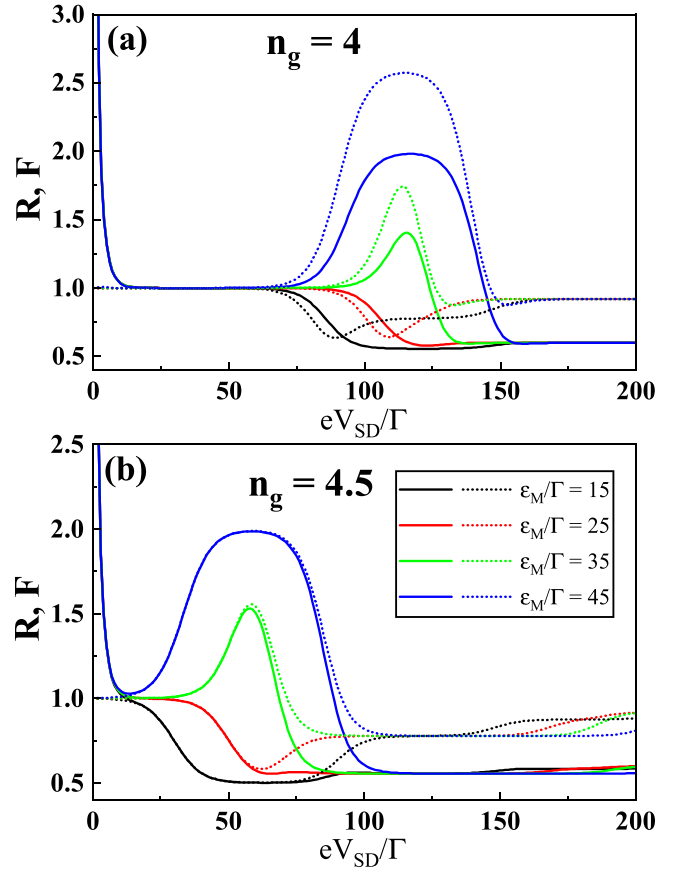

FIG. 7. (a) and (b) Dependence of the randomness parameter (dotted lines) and the Fano factor (solid lines) on the bias voltage with $E_c = 30\Gamma$, $k_B T = 2.5\Gamma$.

as in the setup shown in Fig. 8. To model this non-Majorana device, we take the tight-binding model of the nanowire, and it is given by

$$H = \sum_{i=1}^{L} \epsilon c_i^\dagger c_i + \sum_{i=1}^{L-1} (t c_i^\dagger c_{i+1} + \text{H.c.}), \qquad (35)$$
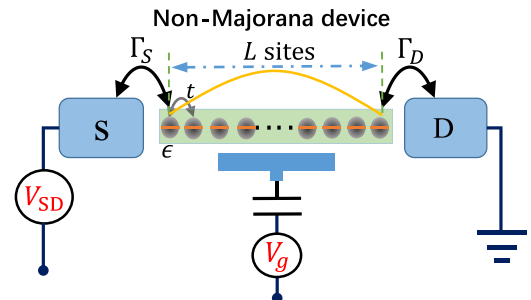

FIG. 8. Schematic of the setup: A nanowire island is modeled as a quantum dot chain of L sites with a global charging energy E_c. In the large-E_c limit, only singly occupied states and the empty state are involved in electron transport. Electrons are injected into (extracted out of) the island through the first (last) site of the chain. The wave function of an eigenstate of the chain spreads over the entire chain, and it takes a finite time for an injected electron to pass through the entire chain.
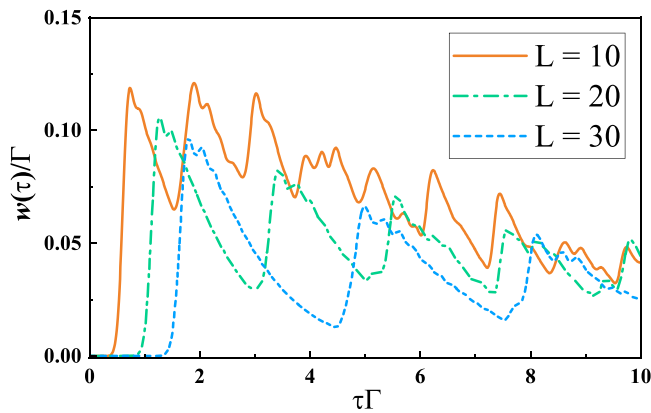
FIG. 9. The WTDs for quantum dot chains of the lengths $L = 10, 20, 30$. The parameters are as follows: $\Gamma_S = \Gamma_D = \Gamma$, $\tilde{\epsilon} = 40\Gamma$, $t = 10\Gamma$. At short times, the WTDs vanish completely for a finite time interval with its width proportional to L.

where ϵ is the on-site energy and t is the hopping. The electrostatic charging energy is described by a term $H_c = E_c(\hat{N} - n_g)^2$ with $\hat{N} = \sum_{i=1}^{L} c_i^\dagger c_i$. For a large E_c, strong Coulomb interaction significantly reduces the number of charge states involved in the electron transport. For simplicity, we assume that the quantum dot chain can accommodate at most one excess electron. In this case, the difference in the charging energy between the empty state and the singly occupied states, denoted by ΔE_c, can be incorporated by redefining the on-site energy $\tilde{\epsilon} = \epsilon + \Delta E_c$.

The WTDs are evaluated by using the generalized master equation approach [30,78], and the results are plotted in Fig. 9. As can be seen from Fig. 9, the WTDs vanish at short times for a finite time interval with its width proportional to L. This occurs because, after an electron tunnels into the drain, it takes a finite time for the subsequent electron to jump into and then travel through the nanowire island. Here, we also notice that the WTDs exhibit complicated oscillatory behaviors. This can be traced back to the quantum coherent processes which allow an electron to hop back and forth multiple times within the chain [78]. Recently, a different approach to tackle the WTD in a free-fermion chain has been developed, and similar results were obtained [78]. Here, the length-dependent suppression and oscillating behaviors of the WTDs are quite different from those of the WTDs associated with electron teleportation induced by MBSs.

IV. CONCLUSION

In summary, we have analyzed the subgap transport and the WTD properties of a Majorana single-charge transistor contacted by two metallic leads. The current, the differential conductance, and the noise Fano factor are calculated by means of the master equation with transition rates obtained from the T-matrix approach. We focused on the effects of the interaction between the Majorana splitting energy and the charging energy on the shot noise and the WTD. For

a pair of Majorana zero modes, the shot noise indicates a sub-Poissonian type for all bias voltages. Differently, a super-Poissonian shot noise generally appears when the Majorana energy splitting is larger than the charging energy. In this case, the energy gap between the first and second excited states becomes smaller than the gap between the ground state and the first excited state. This induces asymmetric tunneling rates between different channels, leading to the dynamical channel blockade effect and super-Poissonian shot noise. With the increase in bias voltage, the shot noise becomes of sub-Poissonian type due to the fact that more energy levels of the island lie in the transport window, which weakens the competition between different transport channels.

Additionally, we considered the WTDs in a Majorana island device and a non-Majorana island device, respectively. At short times, the WTD for electron transport through a nanowire island without MBSs is shown to be completely suppressed for a finite time interval with its width proportional to the length of the island. By contrast, the WTD associated with electron teleportation induced by MBSs has the same form as that in a single-level quantum dot system. In a wider parameter regime, the WTDs are evaluated under a large bias voltage. For a small charging energy, the fluctuation of the Cooper pair number is large in the bias window. The electron from the source can tunnel to the island with no need of overcoming the large charging energy. In this case, the WTDs take a higher finite value at short times. As the charging energy increases, the entrance of an extra electron into the island needs to overcome more charging energy, and levels with higher energy are excluded from the transport window. Correspondingly, the WTDs are suppressed at short times, and the average waiting time becomes longer. We also showed that the Majorana energy splitting can change the WTDs significantly. Furthermore, we found that the randomness parameter matches the Fano factor at low bias voltages. With the increase in the bias voltage, it is shown that there exists a discrepancy between the randomness parameter and the Fano factor as more higher-energy states enter the transport window.

The detection and control of single quanta of charge have been realized in recent experiments using a dynamic single-electron transistor and a Cooper pair splitter [52]. We expect that the detection of particular behaviors of the WTDs in a Majorana island device may be useful in identifying the existence of MBSs. Moreover, the WTDs in the same setup with the island Josephson coupled to another bulk superconductor also deserve further study in this area.

APPENDIX: REGULARIZED COTUNNELING RATES

In this Appendix, we provide detailed derivations of regularized cotunneling rates. Cotunneling processes are described by the next-to-leading term in the T-matrix expansion of H_t. The transition rates are captured by the fourth-order term of H_t in Eq. (7). Here, we take this term and put it into a more refined form as [38]

$$\Gamma_{\alpha\beta,Q'Q} = 2\pi \sum_{i_l,f_l} \left| \langle f_l | \langle Q' | H_{\alpha t} \frac{1}{E_i - H_0 + i0} H_{\beta t} | Q \rangle | i_l \rangle \right|^2 W_{i_\alpha,Q} W_{i_\beta,Q} \delta(E(Q) + \epsilon_{i_l} - E(Q') - \epsilon_{f_l}). \tag{A1}$$

After some algebra, we obtain the elastic cotunneling rates

$$\Gamma_{\alpha,Q}^{(EC)} = \frac{\Gamma_S \Gamma_D}{8\pi} \int d\epsilon\, n_F(\epsilon - \mu_\alpha)[1 - n_F(\epsilon - \mu_{\bar\alpha})] \left| \frac{1}{\epsilon - \Delta E(Q) + i0} - \frac{1}{\epsilon - \Delta E(Q-1) + i0} \right|^2, \tag{A2}$$

where $\Delta E(Q) = E(Q+1) - E(Q) + (-1)^Q \epsilon_M$ and $\bar\alpha$ labels the opposite lead of α. The inelastic cotunneling rates read

$$\Gamma_{\alpha\beta,Q\pm2,Q}^{(AR)} = \frac{1 + \delta_{\alpha,\bar\beta}}{2} \frac{\Gamma_\alpha \Gamma_\beta}{8\pi} \int d\epsilon \int d\epsilon'\, n_F(\pm(\epsilon - \mu_\alpha)) n_F(\pm(\epsilon' - \mu_\beta)) \delta(\epsilon + \epsilon' \mp [E(Q\pm2) - E(Q)])$$

$$\times \left| \frac{1}{\epsilon \mp E_{\mp}(Q) + i0} - \frac{s_\alpha s_\beta}{\epsilon' \mp \Delta E_\pm(Q) + i0} \right|^2, \tag{A3}$$

where $\Delta E_\pm(Q) = E(Q\pm1) - E(Q) + (-1)^Q \epsilon_M$. We note that the expressions for the cotunneling rates in Eqs. (A2) and (A3) are divergent due to the second-order poles contained in the integrands. To get the correct cotunneling rates, a regularization scheme should be applied to eliminate the singularities.

Here, we follow the standard regularization procedure detailed by Refs. [74,79]. This regularization procedure gives us the following two integral formulas:

$$\text{Re} \int d\epsilon \frac{n_F(\epsilon - E_1)[1 - n_F(\epsilon - E_2)]}{(\epsilon - \epsilon_1 - i0)(\epsilon - \epsilon_2 + i0)} = \frac{n_B(E_2 - E_1)}{\epsilon_1 - \epsilon_2} \text{Re}\left\{ \psi\left(\frac{1}{2} + \frac{i\beta}{2\pi}(E_2 - \epsilon_1)\right) - \psi\left(\frac{1}{2} - \frac{i\beta}{2\pi}(E_2 - \epsilon_2)\right) \right.$$

$$\left. - \psi\left(\frac{1}{2} + \frac{i\beta}{2\pi}(E_1 - \epsilon_1)\right) + \psi\left(\frac{1}{2} - \frac{i\beta}{2\pi}(E_1 - \epsilon_2)\right) \right\}, \tag{A4}$$

$$\int d\epsilon \frac{n_F(\epsilon - E_1)[1 - n_F(\epsilon - E_2)]}{|\epsilon - \epsilon_1 + i0|^2} = \frac{\beta n_B(E_2 - E_1)}{2\pi} \text{Im}\left\{ \psi'\left(\frac{1}{2} + \frac{i\beta}{2\pi}(E_2 - \epsilon_1)\right) - \psi'\left(\frac{1}{2} + \frac{i\beta}{2\pi}(E_1 - \epsilon_1)\right) \right\}, \tag{A5}$$

where the divergent parts have been subtracted from the integrals, n_F (n_B) is the Fermi-Dirac (Bose-Einstein) distribution, $\beta = 1/k_B T$, $\psi(x)$ is the digamma function, and $\psi'(x)$ denotes its first derivative. Then, using Eqs. (A4) and (A5), we can directly obtain the regularized cotunneling rates.

[1] S. D. Sarma, M. Freedman, and C. Nayak, Majorana zero modes and topological quantum computation, npj Quantum Inf. **1**, 15001 (2015).

[2] D. Aasen, M. Hell, R. V. Mishmash, A. Higginbotham, J. Danon, M. Leijnse, T. S. Jespersen, J. A. Folk, C. M. Marcus, K. Flensberg, and J. Alicea, Milestones Toward Majorana-Based Quantum Computing, Phys. Rev. X **6**, 031016 (2016).

[3] C. Nayak, S. H. Simon, A. Stern, M. Freedman, and S. Das Sarma, Non-Abelian anyons and topological quantum computation, Rev. Mod. Phys. **80**, 1083 (2008).

[4] J. Alicea, Y. Oreg, G. Refael, F. von Oppen, and M. P. A. Fisher, Non-Abelian statistics and topological quantum information processing in 1D wire networks, Nat. Phys. **7**, 412 (2011).

[5] S. M. Albrecht, A. P. Higginbotham, M. Madsen, F. Kuemmeth, T. S. Jespersen, J. Nygård, P. Krogstrup, and C. M. Marcus, Exponential protection of zero modes in Majorana islands, Nature (London) **531**, 206 (2016).

[6] S. Nadj-Perge, I. K. Drozdov, J. Li, H. Chen, S. Jeon, J. Seo, A. H. MacDonald, B. A. Bernevig, and A. Yazdani, Observation of majorana fermions in ferromagnetic atomic chains on a superconductor, Science **346**, 602 (2014).

[7] P. Fan, F. Yang, G. Qian, H. Chen, Y.-Y. Zhang, G. Li, Z. Huang, Y. Xing, L. Kong, W. Liu, K. Jiang, C. Shen, S. Du, J. Schneeloch, R. Zhong, G. Gu, Z. Wang, H. Ding, and H.-J. Gao, Observation of magnetic adatom-induced Majorana vortex and its hybridization with field-induced Majorana vortex in an iron-based superconductor, Nat. Commun. **12**, 1348 (2021).

[8] L. Kong, S. Zhu, M. Papaj, H. Chen, L. Cao, H. Isobe, Y. Xing, W. Liu, D. Wang, P. Fan, Y. Sun, S. Du, J. Schneeloch, R. Zhong, G. Gu, L. Fu, H.-J. Gao, and H. Ding, Half-integer level shift of vortex bound states in an iron-based superconductor, Nat. Phys. **15**, 1181 (2019).

[9] G. Li, S. Zhu, D. Wang, Y. Wang, and H.-J. Gao, Recent progress of scanning tunneling microscopy/spectroscopy study of Majorana bound states in the FeTe$_{0.55}$Se$_{0.45}$ superconductor, Supercond. Sci. Technol. **34**, 073001 (2021).

[10] S. Zhu, L. Kong, L. Cao, H. Chen, M. Papaj, S. Du, Y. Xing, W. Liu, D. Wang, C. Shen, F. Yang, J. Schneeloch, R. Zhong, G. Gu, L. Fu, Y.-Y. Zhang, H. Ding, and H.-J. Gao, Nearly quantized conductance plateau of vortex zero mode in an iron-based superconductor, Science **367**, 189 (2020).

[11] M. T. Deng, C. L. Yu, G. Y. Huang, M. Larsson, P. Caroff, and H. Q. Xu, Anomalous zero-bias conductance peak in a Nb–InSb nanowire–Nb hybrid device, Nano Lett. **12**, 6414 (2012).

[12] J. Alicea, New directions in the pursuit of Majorana fermions in solid state systems, Rep. Prog. Phys. **75**, 076501 (2012).

[13] A. Haim, E. Berg, F. von Oppen, and Y. Oreg, Signatures of Majorana Zero Modes in Spin-Resolved Current Correlations, Phys. Rev. Lett. **114**, 166406 (2015).

[14] V. Mourik, K. Zuo, S. M. Frolov, S. R. Plissard, E. P. A. M. Bakkers, and L. P. Kouwenhoven, Signatures of Majorana fermions in hybrid superconductor-semiconductor nanowire devices, Science **336**, 1003 (2012).

[15] R. M. Lutchyn, E. P. A. M. Bakkers, L. P. Kouwenhoven, P. Krogstrup, C. M. Marcus, and Y. Oreg, Majorana zero modes in superconductor–semiconductor heterostructures, Nat. Rev. Mater. **3**, 52 (2018).

[16] R. Hützen, A. Zazunov, B. Braunecker, A. L. Yeyati, and R. Egger, Majorana Single-Charge Transistor, Phys. Rev. Lett. **109**, 166403 (2012).

[17] L. Fu, Electron Teleportation via Majorana Bound States in a Mesoscopic Superconductor, Phys. Rev. Lett. **104**, 056402 (2010).

[18] C. Moore, T. D. Stanescu, and S. Tewari, Two-terminal charge tunneling: Disentangling Majorana zero modes from partially separated Andreev bound states in semiconductor-superconductor heterostructures, Phys. Rev. B **97**, 165302 (2018).

[19] C. Moore, C. Zeng, T. D. Stanescu, and S. Tewari, Quantized zero-bias conductance plateau in semiconductor-superconductor heterostructures without topological Majorana zero modes, Phys. Rev. B **98**, 155314 (2018).

[20] M. Valentini, F. Peñaranda, A. Hofmann, M. Brauns, R. Hauschild, P. Krogstrup, P. San-Jose, E. Prada, R. Aguado, and G. Katsaros, Nontopological zero-bias peaks in full-shell nanowires induced by flux-tunable Andreev states, Science **373**, 82 (2021).

[21] S. Das Sarma and H. Pan, Disorder-induced zero-bias peaks in Majorana nanowires, Phys. Rev. B **103**, 195158 (2021).

[22] P. Yu, J. Chen, M. Gomanko, G. Badawy, E. P. A. M. Bakkers, K. Zuo, V. Mourik, and S. M. Frolov, Non-Majorana states yield nearly quantized conductance in proximatized nanowires, Nat. Phys. **17**, 482 (2021).

[23] J.-B. Fu, B. Li, X.-F. Zhang, G.-Z. Yu, G.-Y. Huang, and M.-T. Deng, Experimental review on Majorana zero-modes in hybrid nanowires, Sci. China Phys. Mech. Astron. **64**, 107001 (2021).

[24] D. Wang, J. Wiebe, R. Zhong, G. Gu, and R. Wiesendanger, Spin-Polarized Yu-Shiba-Rusinov States in an Iron-Based Superconductor, Phys. Rev. Lett. **126**, 076802 (2021).

[25] D. A. Bagrets and Yu. V. Nazarov, Full counting statistics of charge transfer in Coulomb blockade systems, Phys. Rev. B **67**, 085316 (2003).

[26] V. F. Maisi, D. Kambly, C. Flindt, and J. P. Pekola, Full Counting Statistics of Andreev Tunneling, Phys. Rev. Lett. **112**, 036801 (2014).

[27] P. Stegmann, J. König, and S. Weiss, Coherent dynamics in stochastic systems revealed by full counting statistics, Phys. Rev. B **98**, 035409 (2018).

[28] P. Stegmann and J. König, Short-time counting statistics of charge transfer in Coulomb-blockade systems, Phys. Rev. B **94**, 125433 (2016).

[29] K. Ptaszyński, Waiting time distribution revealing the internal spin dynamics in a double quantum dot, Phys. Rev. B **96**, 035409 (2017).

[30] K. H. Thomas and C. Flindt, Electron waiting times in non-Markovian quantum transport, Phys. Rev. B **87**, 121405(R) (2013).

[31] G.-M. Tang, F. Xu, and J. Wang, Waiting time distribution of quantum electronic transport in the transient regime, Phys. Rev. B **89**, 205310 (2014).

[32] R. Seoane Souto, R. Avriller, R. C. Monreal, A. Martín-Rodero, and A. Levy Yeyati, Transient dynamics and waiting time distribution of molecular junctions in the polaronic regime, Phys. Rev. B **92**, 125435 (2015).

[33] M. Albert, D. Chevallier, and P. Devillard, Waiting times of entangled electrons in normal–superconducting junctions, Phys. E (Amsterdam) **76**, 209 (2016).

[34] G. Tang, F. Xu, S. Mi, and J. Wang, Spin-resolved electron waiting times in a quantum-dot spin valve, Phys. Rev. B **97**, 165407 (2018).

[35] S. L. Rudge and D. S. Kosov, Counting quantum jumps: A summary and comparison of fixed-time and fluctuating-time statistics in electron transport, J. Chem. Phys. **151**, 034107 (2019).

[36] T. Brandes, Waiting times and noise in single particle transport, Ann. Phys. (Berlin) **17**, 477 (2010).

[37] N. S. Davis, S. L. Rudge, and D. S. Kosov, Electronic statistics on demand: Bunching, antibunching, positive, and negative correlations in a molecular spin valve, Phys. Rev. B **103**, 205408 (2021).

[38] S. L. Rudge and D. S. Kosov, Distribution of waiting times between electron cotunneling events, Phys. Rev. B **98**, 245402 (2018).

[39] W. Liu, F. Wang, and R. Liang, Waiting time distributions of transport through a two-channel quantum system, Appl. Sci. **10**, 1772 (2020).

[40] D. S. Kosov, Waiting time between charging and discharging processes in molecular junctions, J. Chem. Phys. **149**, 164105 (2018).

[41] N. Walldorf, C. Padurariu, A.-P. Jauho, and C. Flindt, Electron Waiting Times of a Cooper Pair Splitter, Phys. Rev. Lett. **120**, 087701 (2018).

[42] K. Wrześniewski and I. Weymann, Current cross-correlations and waiting time distributions in Andreev transport through Cooper pair splitters based on a triple quantum dot system, Phys. Rev. B **101**, 155409 (2020).

[43] N. Walldorf, F. Brange, C. Padurariu, and C. Flindt, Noise and full counting statistics of a Cooper pair splitter, Phys. Rev. B **101**, 205422 (2020).

[44] M. Albert, G. Haack, C. Flindt, and M. Büttiker, Electron Waiting Times in Mesoscopic Conductors, Phys. Rev. Lett. **108**, 186806 (2012).

[45] G. Haack, M. Albert, and C. Flindt, Distributions of electron waiting times in quantum-coherent conductors, Phys. Rev. B **90**, 205429 (2014).

[46] S. Mi, P. Burset, and C. Flindt, Electron waiting times in hybrid junctions with topological superconductors, Sci. Rep. **8**, 16828 (2018).

[47] M. Albert, D. Chevallier, and P. Devillard, Waiting times of entangled electrons in normal–superconducting junctions, Phys. E (Amsterdam) **82**, 85 (2016).

[48] M. Albert and P. Devillard, Waiting time distribution for trains of quantized electron pulses, Phys. Rev. B **90**, 035431 (2014).

[49] P. Stegmann, B. Sothmann, J. König, and C. Flindt, Electron Waiting Times in a Strongly Interacting Quantum Dot: Interaction Effects and Higher-Order Tunneling Processes, Phys. Rev. Lett. **127**, 096803 (2021).

[50] M. Jenei, E. Potanina, R. Zhao, K. Y. Tan, A. Rossi, T. Tanttu, K. W. Chan, V. Sevriuk, M. Möttönen, and A. Dzurak, Waiting time distributions in a two-level fluctuator coupled to a superconducting charge detector, Phys. Rev. Res. **1**, 033163 (2019).

[51] F. Brange, A. Schmidt, J. C. Bayer, T. Wagner, C. Flindt, and R. J. Haug, Controlled emission time statistics of a dynamic single-electron transistor, Sci. Adv. **7**, eabe0793 (2021).

[52] A. Ranni, F. Brange, E. T. Mannila, C. Flindt, and V. F. Maisi, Real-time observation of Cooper pair splitting showing strong non-local correlations, Nat. Commun. **12**, 6358 (2021).

[53] S. Gustavsson, R. Leturcq, M. Studer, I. Shorubalko, T. Ihn, K. Ensslin, D.C. Driscoll, and A.C. Gossard, Electron counting in quantum dots, Surf. Sci. Rep. **64**, 191 (2009).

[54] C. Bäuerle, D. C. Glattli, T. Meunier, F. Portier, P. Roche, P. Roulleau, S. Takada, and X. Waintal, Coherent control of single electrons: a review of current progress, Rep. Prog. Phys. **81**, 056503 (2018).

[55] S. Gustavsson, M. Studer, R. Leturcq, T. Ihn, K. Ensslin, D. C. Driscoll, and A. C. Gossard, Detecting single-electron tunneling involving virtual processes in real time, Phys. Rev. B **78**, 155309 (2008).

[56] A. Kurzmann, P. Stegmann, J. Kerski, R. Schott, A. Ludwig, A. D. Wieck, J. König, A. Lorke, and M. Geller, Optical Detection of Single-Electron Tunneling into a Semiconductor Quantum Dot, Phys. Rev. Lett. **122**, 247403 (2019).

[57] Y.-H. Lai, S. Das Sarma, and J. D. Sau, Theory of Coulomb blockaded transport in realistic Majorana nanowires, Phys. Rev. B **104**, 085403 (2021).

[58] C.-K. Chiu, J. D. Sau, and S. Das Sarma, Conductance of a superconducting Coulomb-blockaded Majorana nanowire, Phys. Rev. B **96**, 054504 (2017).

[59] A. Golub and B. Horovitz, Shot noise in a Majorana fermion chain, Phys. Rev. B **83**, 153415 (2011).

[60] J. Ulrich and F. Hassler, Majorana-assisted nonlocal electron transport through a floating topological superconductor, Phys. Rev. B **92**, 075443 (2015).

[61] H.-F. Lü, H.-Z. Lu, and S.-Q. Shen, Nonlocal noise cross correlation mediated by entangled Majorana fermions, Phys. Rev. B **86**, 075318 (2012).

[62] H.-F. Lü, H.-Z. Lu, and S.-Q. Shen, Enhanced current noise correlations in a Coulomb-Majorana device, Phys. Rev. B **93**, 245418 (2016).

[63] J. Liu, A. C. Potter, K. T. Law, and P. A. Lee, Zero-Bias Peaks in the Tunneling Conductance of Spin-Orbit-Coupled Superconducting Wires with and without Majorana End-States, Phys. Rev. Lett. **109**, 267002 (2012).

[64] S. Vaitiekėnas, G. W. Winkler, B. van Heck, T. Karzig, M.-T. Deng, K. Flensberg, L. I. Glazman, C. Nayak, P. Krogstrup, R. M. Lutchyn, and C. M. Marcus, Flux-induced topological superconductivity in full-shell nanowires, Science **367**, eaav3392 (2020).

[65] S. Das Sarma, J. D. Sau, and T. D. Stanescu, Splitting of the zero-bias conductance peak as smoking gun evidence for the existence of the Majorana mode in a superconductor-semiconductor nanowire, Phys. Rev. B **86**, 220506(R) (2012).

[66] A. Zazunov, A. L. Yeyati, and R. Egger, Coulomb blockade of Majorana-fermion-induced transport, Phys. Rev. B **84**, 165440 (2011).

[67] K. Flensberg, Tunneling characteristics of a chain of Majorana bound states, Phys. Rev. B **82**, 180516(R) (2010).

[68] K. Kaasbjerg and W. Belzig, Full counting statistics and shot noise of cotunneling in quantum dots and single-molecule transistors, Phys. Rev. B **91**, 235413 (2015).

[69] C. Timm, Tunneling through molecules and quantum dots: Master-equation approaches, Phys. Rev. B **77**, 195416 (2008).

[70] H.-F. Lü, H.-Z. Lu, and S.-Q. Shen, Current noise cross correlation mediated by Majorana bound states, Phys. Rev. B **90**, 195404 (2014).

[71] M. Albert, C. Flindt, and M. Büttiker, Distributions of Waiting Times of Dynamic Single-Electron Emitters, Phys. Rev. Lett. **107**, 086805 (2011).

[72] Y. M. Blanter and M. Buttiker, Shot noise in mesoscopic conductors, Phys. Rep. **336**, 1 (2000).

[73] W. Belzig, Full counting statistics of super-Poissonian shot noise in multilevel quantum dots, Phys. Rev. B **71**, 161301(R) (2005).

[74] J. Koch, F. von Oppen, and A. V. Andreev, Theory of the Franck-Condon blockade regime, Phys. Rev. B **74**, 205438 (2006).

[75] K. Ptaszyński, Nonrenewal statistics in transport through quantum dots, Phys. Rev. B **95**, 045306 (2017).

[76] K. Ptaszyński, First-passage times in renewal and nonrenewal systems, Phys. Rev. E **97**, 012127 (2018).

[77] A. A. Budini, Large deviations of ergodic counting processes: A statistical mechanics approach, Phys. Rev. E **84**, 011141 (2011).

[78] G. T. Landi, Waiting time statistics in boundary-driven free fermion chains, Phys. Rev. B **104**, 195408 (2021).

[79] J. Koch, F. von Oppen, Y. Oreg, and E. Sela, Thermopower of single-molecule devices, Phys. Rev. B **70**, 195107 (2004).